

Optimized U-Net for Brain Tumor Segmentation

Michał Futrega, Alexandre Milesi, Michał Marcinkiewicz, Pablo Ribalta

NVIDIA, Santa Clara CA 95051, USA
 {mfutrega,alexandrem,michalm,pribalta}@nvidia.com

Abstract. We propose an optimized U-Net architecture for a brain tumor segmentation task in the BraTS21 Challenge. To find the optimal model architecture and learning schedule we ran an extensive ablation study to test: deep supervision loss, Focal loss, decoder attention, drop block, and residual connections. Additionally, we have searched for the optimal depth of the U-Net and number of convolutional channels. Our solution was the winner of the challenge validation phase, with the normalized statistical ranking score of 0.267 and mean Dice score of 0.8855.

Keywords: U-Net · Brain Tumor Segmentation · Deep Learning · MRI

1 Introduction

One of the most challenging problems in medical image processing is automatic brain tumor segmentation. Obtaining a computational model capable of surpassing a trained human-level performance would provide valuable assistance to clinicians and would enable a more precise, reliable, and standardized approach to disease detection, treatment planning and monitoring. Gliomas are the most common type of brain tumors in humans [1]. Their accurate segmentation is a challenging medical image analysis task due to their variable shape and appearance in multi-modal magnetic resonance imaging (MRI). Manual segmentation of such brain tumors requires a great deal of medical expertise, is time-consuming, and prone to human error. Moreover, the manual process lacks consistency and reproducibility, which negatively affects the results and can ultimately lead to incorrect prognosis and treatment.

The rapid progress in development of deep learning (DL) algorithms shows great potential for application of deep neural networks (DNNs) in computer-aided automatic or semi-automatic methods for medical data analysis. The drastic improvements of convolutional neural networks (CNNs) resulted in models being able to approach or surpass the human level performance in plethora of applications, such as image classification [2] or microscope image segmentation [3], among many others. DL-based models are great candidates for brain tumor segmentation, as long as sufficient amount of training data is supplied. The Brain Tumor Segmentation Challenge (BraTS) provides a large, high-quality dataset consisting of multi-modal MRI brain scans with corresponding segmentation masks [4,5,6,7].

Training a performant and accurate DL-based model requires, besides a high-quality dataset, a carefully designed DNN to learn from the data and capture all the relevant information. This task usually requires a lot of experience and a trial-and-error approach. The state-of-the-art models in brain tumor segmentation are based on an encoder-decoder architectures, with U-Net [8] being the most popular for medical image segmentation, based on number of citations. In the recent years, U-Net-like architectures were among top submissions to the BraTS challenge. For instance, in 2018, Myronenko *et al.*, modified a U-Net model by adding a variational autoencoder branch for regularization [9]. In 2019, Jiang *et al.*, employed a two-stage U-Net pipeline to segment the substructures of brain tumors from coarse to fine [10]. In 2020, Isensee *et al.*, applied the nnU-Net framework [11] with specific BraTS designed modifications regarding data post-processing, region-based training, data augmentation, and minor modifications to the nnU-Net pipeline [12].

Those achievements prove that a well-designed U-Net-based architecture has the ability to perform very well on tasks such as brain tumor segmentation. However, in most cases, there is a need for manual effort of an expert to design and apply required modifications to the baseline model. In this context, the winning model of BraTS20, namely nnU-Net, represents a paramount step towards automated DNN design. The nnU-Net represents a framework for training (medical) segmentation models. The framework is able to adapt the model architecture and data pipeline to the given task.

In this paper, we propose a solution for BraTS21 challenge, with goal to make it accurate, robust and GPU efficient. Our starting point was NVIDIA the implementation [13] of the nnU-Net framework [11], which we optimized further. Our solution has won the challenge validation phase, with the normalized statistical ranking score of 0.267.

In Section 2, we describe our method i.e., data pre-processing and augmentations, modified U-Net architecture and inference with post-processing. Next, in Section 3, we present experimental results based on which we selected the final model architecture. In the last Section, 4 we present and discuss our conclusions based on our participation in the BraTS21 challenge.

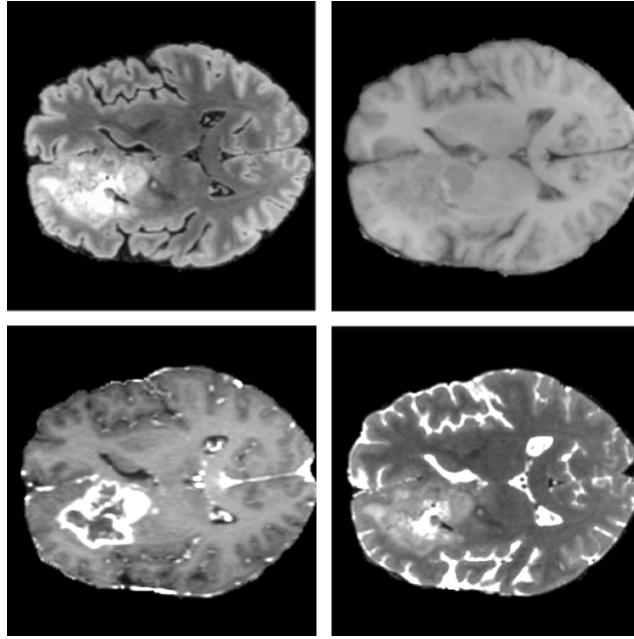


Fig. 1. Visualization of a BraTS2021_000000 example from the training dataset. Each plot presents a different modality (from top left to bottom right: FLAIR, T1, T1Gd, T2).

2 Method

2.1 Data

The training dataset provided for the BraTS21 challenge [4,5,6,7] consists of 1,251 brain MRI scans along with segmentation annotations of tumorous regions. The 3D volumes were skull-stripped and resampled to 1 mm^3 isotropic resolution, with dimensions of (240, 240, 155) voxels. For each example, four modalities were given: native (T1), post-contrast T1-weighted (T1Gd), T2-weighted (T2), and T2 Fluid Attenuated Inversion Recovery (T2-FLAIR). Example images of each modality are presented on Fig. 3. Segmentation labels were annotated manually by one to four experts. Annotations consist of four classes: enhancing tumor (ET), peritumoral edematous tissue (ED), necrotic tumor core (NCR), and background (voxels that are not part of the tumor).

2.2 Data pre-processing and augmentation

Each example of the BraTS21 dataset consists of four NIfTI [14] files with different MRI modalities. As a first step of data pre-processing, all four modalities were stacked such that each example has shape (4, 240, 240, 155) (input tensor is

in the (C, H, W, D) layout, where C-channels, H-height, W-width and D-depth). Then redundant background voxels (with voxel value zero) on the borders of each volume were cropped, as they do not provide any useful information and can be ignored by the neural network. Subsequently, for each example, the mean and the standard deviation were computed within the non-zero region for each channel separately. All volumes were normalized by first subtracting the mean and then divided by the standard deviation. The background voxels were not normalized so that their value remained at zero. To distinguish between background voxels and normalized voxels which have values close to zero, an additional input channel was created with one-hot encoding for foreground voxels and stacked with the input data.

Data augmentation is a technique that alleviates the overfitting problem by artificially extending a dataset during the training phase. To make our method more robust, the following data augmentations were used during training phase:

1. **Biased crop:** From the input volume, a patch of dimensions (5, 128, 128, 128) was randomly cropped. Additionally, with probability of 0.4 the patch selected via random biased crop is guaranteed that some foreground voxels (with positive class in the ground truth) are present in the cropped region.
2. **Flips:** With probability of 0.5, for each x, y, z axis independently, volume was flipped along that axis.
3. **Gaussian Noise:** With probability of 0.15, random Gaussian noise with mean zero and standard deviation sampled uniformly from (0, 0.33) is sampled for each voxel and added to the input volume.
4. **Gaussian Blur:** With probability of 0.15, Gaussian blurring with standard deviation of the Gaussian Kernel sampled uniformly from (0.5, 1.5) is applied to the input volume.
5. **Brightness:** With probability of 0.15, a random value is sampled uniformly from (0.7, 1.3) and then input volume voxels are multiplied by it.

The data loading pipeline was implemented with NVIDIA Data Loading Library (DALI) ¹.

2.3 Model

We have tested vanilla U-Net [8] as a baseline model together with its two modifications: UNETR and residual U-Net with autoencoder regularization (SegResNetVAE). The UNETR [15] model is a generalization of Vision Transformer (ViT) [16] to the 3D convolutions—it replaces the 3D convolutions in the encoder with multi-head self attention [17]. The residual U-Net with autoencoder regularization (SegResNetVAE) has won the BraTS 2018 challenge and extends U-Net architecture with variational autoencoder (VAE) [18] branch in the decoder, which reconstructs the input and has a regularization effect.

¹ <https://docs.nvidia.com/deeplearning/dali/user-guide/docs/index.html>

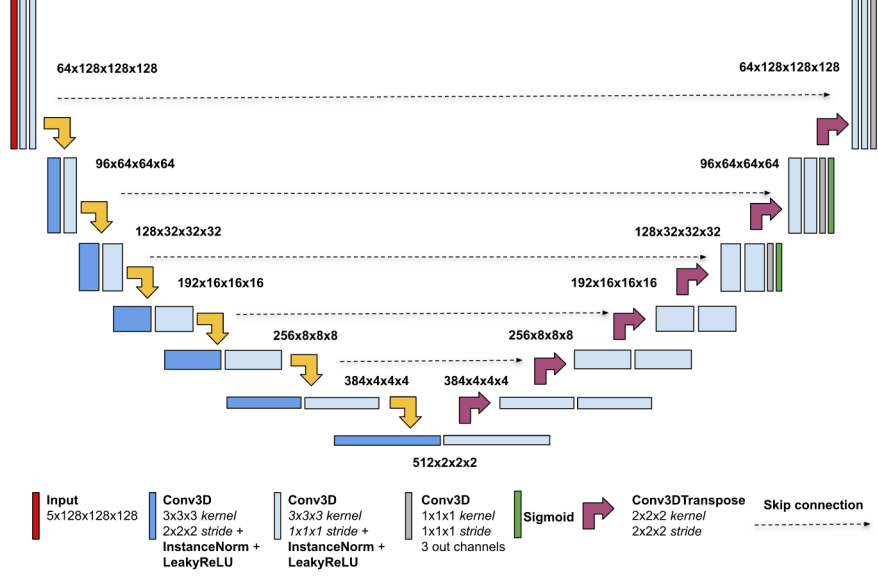


Fig. 2. Selected U-Net architecture. The encoder transforms input volume until it reaches a size of $2 \times 2 \times 2$ in the bottleneck. Then the decoder upsamples it with transposed convolutions back to the original input shape of $128 \times 128 \times 128$. Additional two output heads are used for deep supervision loss.

Based on our experiments (the detailed results are shown in subsection 3.3), a baseline U-Net achieves the best results, and was selected for further exploration. The next optimization was adjusting the encoder depth and optimal selection of the convolution channels. As a baseline, a default U-Net architecture from the nnU-Net framework² was used, i.e., the depth of the network was 6, and the convolution channels at each encoder level were: 32, 64, 128, 256, 320, 320. Our experiments have demonstrated that increasing the depth of the encoder to 7, and modifying the number of channels to: 64, 96, 128, 192, 256, 384, 512, further improves the baseline score.

We have also experimented with various U-Net architecture modifications, namely deep supervision [19], decoder attention [20], residual connections [21], and drop block [22]. However, deep supervision was the only modification that considerably improved the mean Dice score over the baseline model.

For deep supervision, we used two additional output heads at the decoder levels with feature map sizes $(64, 64, 64)$ and $(32, 32, 32)$. To match the shape of the additional predictions with the label shape of $(128, 128, 128)$ we downsampled the label using the nearest neighbor interpolation to the $(64, 64, 64)$ and $(32, 32, 32)$ shapes, so that loss can be computed for additional outputs.

² <https://github.com/NVIDIA/DeepLearningExamples/tree/master/PyTorch/Segmentation/nnUNet>

The final architecture is shown in the Fig. 2. The input volume of shape $5 \times 128 \times 128 \times 128$ is first processed by an input block with two convolution layers with kernel $3 \times 3 \times 3$ and stride $1 \times 1 \times 1$, together with instance normalization and LeakyReLU activation (with negative slope set to 0.01) such that the feature map has 64 channels and spatial dimensions $128 \times 128 \times 128$.

Then the feature map is transformed by six downsampling blocks, where each first convolution reduces the spatial dimensions of the feature map by a factor of two via convolution layers with kernel size $3 \times 3 \times 3$ and stride $2 \times 2 \times 2$. The reduced feature maps are then refined by convolution layers with kernel size $3 \times 3 \times 3$ and stride $1 \times 1 \times 1$. Downsampled feature maps have a size of $512 \times 2 \times 2 \times 2$ at the bottleneck and then their spatial dimensions are increased by six upsampling blocks which consist of transposed convolutions with kernel size $2 \times 2 \times 2$ and stride $2 \times 2 \times 2$ that doubles the spatial dimensions of the feature maps and two convolutions. After the feature map is upsampled to the input volume size, it is processed by a convolution with a $1 \times 1 \times 1$ kernel, $1 \times 1 \times 1$ stride followed by sigmoid activation. The final output feature map has 3 output channels where each channel corresponds to a different class (ET, TC, WT).

2.4 Loss function

Based on the *nnU-Net for Brain Tumor Segmentation* [12] paper, the classes present in the label were converted to the three partially overlapping regions: whole tumor (classes 1, 2, 4), tumor core (classes 1, 4) and enhancing tumor (class 4). The contest leaderboard is computed based on those overlapping regions instead of classes present in the labels, thus it is beneficial to construct the loss function based on classes used for ranking calculation.

Each region was optimized separately with a sum of binary cross-entropy or Focal loss [23] (with gamma parameter set to 2) with the Dice loss [24]. For Dice loss, its batched variant was used, i.e., Dice loss was computed over all samples in the batch instead of averaging the Dice loss over each sample separately.

To compute the deep supervision loss, labels were first downsampled using nearest neighbor interpolation to the $(64, 64, 64)$ and $(32, 32, 32)$ spatial shapes such that they match the shapes of additional outputs. For labels y_i and predictions p_i for $i = 1, 2, 3$, where $i = 1$ corresponds to the last output head, $i = 2$ is the output head on the penultimate decoder level and $i = 3$ is before the penultimate, final loss function is computed as follows:

$$\mathcal{L}(y_1, y_2, y_3, p_1, p_2, p_3) = \mathcal{L}(y_1, p_1) + \frac{1}{2}\mathcal{L}(y_2, p_2) + \frac{1}{4}\mathcal{L}(y_3, p_3). \quad (1)$$

2.5 Inference

During inference, the input volume can have arbitrary size, instead of the fixed patch size $(128, 128, 128)$ as during the training phase. Thus, we used a sliding window inference³, where the window has the same size as the training patch,

³ MONAI [sliding window implementation](#) was used.

i.e., $(128, 128, 128)$ and adjacent windows overlap by half the size of a patch. The predictions on the overlapping regions are then averaged with Gaussian importance weighting, such that the weights of the center voxels have higher importance, as in the original nnU-Net paper [11].

One of the known ways to improve robustness of predictions is to apply test time augmentations. During inference, we have created eight versions of the input volume, such that each version corresponds to one of eight possible flips along the x, y, z axis combination. Then we run inference for each version of the input volume and transform the predictions back to the original input volume orientation by applying the same flips to predictions as was used for the input volume. Finally, the probabilities from all predictions were averaged.

By optimizing the three overlapping regions (ET, TC, WT) we had to convert them back to the original classes (NCR, ED, ET). The strategy for transforming classes back to the original one is the following: if the WT probability for a given voxel is less than 0.45 then its class is set to 0 (background), otherwise if the probability for TC is less than 0.4 the voxel class is 2 (ED), and finally if probability for ET is less than 0.45 voxel has class 1 (NCR), or otherwise 4 (ET).

Furthermore, we applied the following post-processing strategy: find ET connected components, for components smaller than 16 voxels with mean probability smaller than 0.9, replace their class to NCR (such that voxels are still considered part of the tumor core), next if there is overall less than 73 voxels with ET and their mean probability is smaller than 0.9 replace all ET voxels to NCR. With such post-processing we avoided the edge case where the model predicted a few voxels with enhancing tumor (ET) but there were not any in the ground truth. Such post-processing was beneficial to the final score as if there were no enhancing tumor voxels in the label, then the Dice score for zero false positive prediction was 1, and 0 otherwise.

3 Results

3.1 Implementation

Our solution is written in PyTorch [25] and extends NVIDIA’s implementation of the nnU-Net. The code is publicly available on the NVIDIA Deep Learning Examples GitHub repository⁴. Proposed solution is using the NVIDIA NGC PyTorch 21.07 Docker container⁵ which allows for the full encapsulation of dependencies, reproducible runs, as well as easy deployment on any system. All training and inference runs were performed with use of Mixed Precision [26], which speeds-up the model and reduces the GPU memory consumption. Experiments were run on NVIDIA DGX A100 ($8 \times A100$ 80 GB) system.⁶

⁴ <https://github.com/NVIDIA/DeepLearningExamples/tree/master/PyTorch/Segmentation/nnUNet>

⁵ <https://ngc.nvidia.com/catalog/containers/nvidia:pytorch>

⁶ <https://www.nvidia.com/en-us/data-center/a100>

3.2 Training schedule

Each experiment was trained for 1,000 epochs using the Adam optimizer [27] with three different learning rates: 0.0005, 0.0007, 0.0009 and a weight decay equal to 0.0001. Additionally, during the first 1000 steps, we used a linear warm-up of the learning rate and then decreased it with a cosine annealing scheduler [28].

For models evaluation, we used 5-fold cross validation and compare the average of the highest Dice score reached on each of the 5-folds. The evaluation on the validation set was run after every epoch. For each fold we have stored the two checkpoints with the highest mean Dice score on validation set reached during the training phase. Then during the inference phase, we ensembled the predictions from stored checkpoints by averaging the probabilities.

3.3 Experiments

To select the model architecture, we experimented with three U-Net variants: baseline U-Net [8] which architecture follows the nnU-Net [11] architecture heuristic, UNETR [15] which replaces the U-Net encoder with a Vision Transformer (ViT) [16] generalization for the 3D convolutions, and U-Net with autoencoder regularization (SegResNetVAE) which extends U-Net architecture with variational autoencoder (VAE) [18] branch for input reconstruction in the decoder.

Model	U-Net	UNETR	SegResNetVAE
Fold 0	0.9087	0.9044	0.9086
Fold 1	0.9100	0.8976	0.9090
Fold 2	0.9162	0.9051	0.9140
Fold 3	0.9238	0.9111	0.9219
Fold 4	0.9061	0.8971	0.9053
Mean Dice	0.9130	0.9031	0.9118

Table 1. Averaged Dice scores of ET, TC, WT classes for each 5-folds comparing the baseline U-Net, UNETR, SegResNetVAE models.

Presented results in the Table 1 have shown that baseline U-Net achieves the highest score. Although the score of SegResNetVAE is similar to the plain U-Net, the training time is three times longer comparing to U-Net, because of the additional VAE branch. Thus, we decided to select U-Net architecture for further exploration.

In the next phase of experiments we tested various U-Net architecture tweaks: decoder attention [20], deep supervision [19], residual connections [21] and drop block [22]. Additionally, we have experimented with a the modified loss function with Focal loss [23] instead of cross-entropy, so that the loss function was Focal+Dice.

The experimental results presented in the Table 2 have shown that the only extension which significantly improves the 5-fold average Dice score over the baseline U-Net (0.9130) was the deep supervision (0.9149).

Model	baseline	Attention	DS	Residual	DB	Focal
Fold 0	0.9087	0.9091	0.9111	0.9087	0.9096	0.9094
Fold 1	0.9100	0.9110	0.9115	0.9103	0.9114	0.9026
Fold 2	0.9162	0.9157	0.9175	0.9175	0.9159	0.9146
Fold 3	0.9238	0.9232	0.9268	0.9233	0.9241	0.9229
Fold 4	0.9061	0.9061	0.9074	0.9070	0.9071	0.9072
Mean Dice	0.9130	0.9130	0.9149	0.9134	0.9136	0.9133

Table 2. Averaged Dice scores of ET, TC, WT classes for each 5-folds comparing the decoder attention (Attention), deep supervision (DS), residual connections (Residual), drop block (DB) and Focal loss (Focal).

Finally, for the U-Net with deep supervision, we tested the modification of the U-Net encoder. The baseline U-Net architecture follows the architecture heuristic from the nnU-Net [11] framework for which the depth of the network was 6, and the convolution channels at each encoder level was: 32, 64, 128, 256, 320, 320. We experimented with encoder of depth 7, modified the number of channels to: 64, 96, 128, 192, 256, 384, 512, and checked the input volume with additional channel with one-hot encoding for foreground voxels.

Model	DS	Deeper	Channels	One-hot	D+C+O
Fold 0	0.9111	0.9118	0.9107	0.9109	0.9118
Fold 1	0.9115	0.9140	0.9135	0.9132	0.9141
Fold 2	0.9175	0.9170	0.9173	0.9174	0.9176
Fold 3	0.9268	0.9256	0.9265	0.9263	0.9268
Fold 4	0.9074	0.9079	0.9072	0.9075	0.9076
Mean Dice	0.9149	0.9152	0.9150	0.9050	0.9156

Table 3. Averaged Dice scores of ET, TC, WT classes for each 5-folds comparing the deep supervision (DS), deeper U-Net encoder, modified number of convolution channels, additional input channel with one-hot encoding for foreground voxels, and all modification applied together (D+C+O) i.e., deeper U-Net with changed number of convolution channels and one-hot encoding channel for foreground voxels.

The results in the Table 3 have shown that applying each of the modification separately is slightly improving the score over baseline U-Net with deep supervision (0.9149), however if using all modification together then the score is further improved (0.9156).

Finally, we experimented with a post-processing strategy. It is known from previous BraTS edition that removing small regions with enhanced tumor can be beneficial to the final score. It is so because if there is no enhancing tumor in the label, then the Dice score for zero false positive prediction is 1, and 0 otherwise. The best strategy we found for our 5-fold cross-validation is the following: find ET connected components, for components smaller than 16 voxels with mean probability smaller than 0.9, replace their class to NCR, next if there is overall less than 73 voxels with ET and their mean probability is smaller than 0.9 replace all ET voxels to NCR.

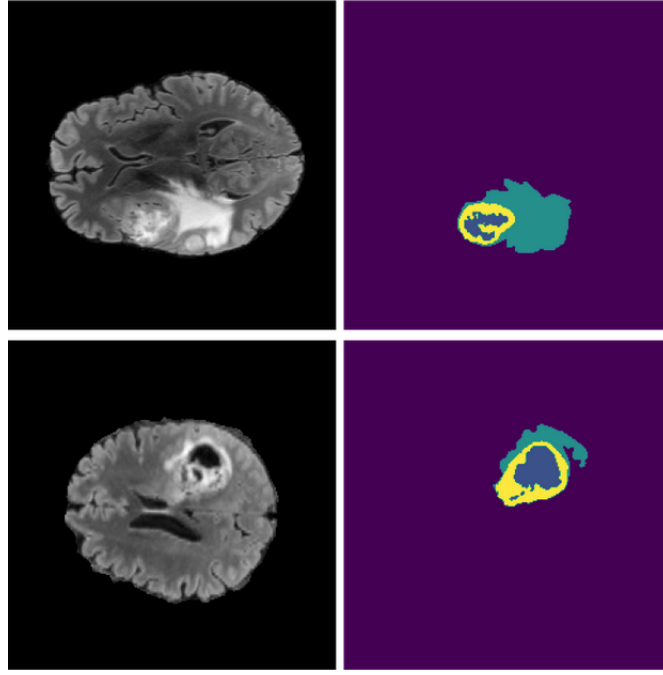


Fig. 3. Predictions on the challenge validation dataset. On the left column FLAIR modality is visualized while on the right model predictions where the meaning of colors is the following: purple - background, blue - NCR, turquoise - ED, yellow - ET.

Post-processing	without	with
Fold 0	0.9118	0.9132
Fold 1	0.9141	0.9142
Fold 2	0.9176	0.9189
Fold 3	0.9268	0.9268
Fold 4	0.9076	0.9086
Mean Dice	0.9156	0.9163

Table 4. Averaged Dice scores of ET, TC, WT classes for each 5-folds without and with post-processing.

The best model, i.e., deeper U-Net with deep supervision, modified number of channels and additional input one-hot encoding channel for foreground voxels was the winner of challenge validation phase. The detailed scores are shown in the Table 5.

1	2	3	4	5	6	7	8	9
0.267	0.272	0.287	0.289	0.298	0.305	0.306	0.312	0.316

Table 5. Top 9 normalized statistical ranking scores for BraTS21 validation phase.

4 Conclusions

We have experimented with various U-Net variants (U-Net [8], UNETR [15] and SegResNetVAE [9]), architecture modifications and training schedule tweaks like: decoder attention [20], deep supervision [19], drop block [22], residual connections [21], Focal loss [23]. Based on our experiments, U-Net with deep supervision yields the best results which can be further improved by adding additional input channel with one-hot encoding for foreground, increasing encoder depth together with number of convolutional channels and post-processing.

References

1. Goodenberger, M.L., Jenkins, R.B.: Genetics of adult glioma. *Cancer Genetics* **205** (12 2012). <https://doi.org/10.1016/j.cancergen.2012.10.009>
2. Russakovsky, O., Deng, J., Su, H., Krause, J., Satheesh, S., Ma, S., Huang, Z., Karpathy, A., Khosla, A., Bernstein, M., Berg, A.C., Fei-Fei, L.: ImageNet Large Scale Visual Recognition Challenge. *International Journal of Computer Vision* **115** (12 2015). <https://doi.org/10.1007/s11263-015-0816-y>
3. Zeng, T., Wu, B., Ji, S.: DeepEM3D: approaching human-level performance on 3D anisotropic EM image segmentation. *Bioinformatics* **33**(16), 2555–2562 (03 2017). <https://doi.org/10.1093/bioinformatics/btx188>, <https://doi.org/10.1093/bioinformatics/btx188>
4. Baid, U., Ghodasara, S., Bilello, M., Mohan, S., Calabrese, E., Colak, E., Farahani, K., Kalpathy-Cramer, J., Kitamura, F.C., Pati, S., Prevedello, L.M., Rudie, J.D., Sako, C., Shinohara, R.T., Bergquist, T., Chai, R., Eddy, J., Elliott, J., Reade, W., Schaffter, T., Yu, T., Zheng, J., Annotators, B., Davatzikos, C., Mongan, J., Hess, C., Cha, S., Villanueva-Meyer, J., Freymann, J.B., Kirby, J.S., Wiestler, B., Crivellaro, P., Colen, R.R., Kotrotsou, A., Marcus, D., Milchenko, M., Nazeri, A., Fathallah-Shaykh, H., Wiest, R., Jakab, A., Weber, M.A., Mahajan, A., Menze, B., Flanders, A.E., Bakas, S.: The RSNA-ASNR-MICCAI BraTS 2021 Benchmark on Brain Tumor Segmentation and Radiogenomic Classification (2021)
5. Menze, B.H., Jakab, A., Bauer, S., Kalpathy-Cramer, J., Farahani, K., Kirby, J., Burren, Y., Porz, N., Slotboom, J., Wiest, R., Lanczi, L., Gerstner, E., Weber, M.A., Arbel, T., Avants, B.B., Ayache, N., Buendia, P., Collins, D.L., Cordier, N., Corso, J.J., Criminisi, A., Das, T., Delingette, H., Demiralp, C., Durst, C.R., Dojat, M., Doyle, S., Festa, J., Forbes, F., Geremia, E., Glocker, B., Golland, P., Guo, X., Hamamci, A., Iftekharuddin, K.M., Jena, R., John, N.M., Konukoglu, E., Lashkari, D., Mariz, J.A., Meier, R., Pereira, S., Precup, D., Price, S.J., Raviv, T.R., Reza, S.M.S., Ryan, M., Sarikaya, D., Schwartz, L., Shin, H.C., Shotton, J., Silva, C.A., Sousa, N., Subbanna, N.K., Szekely, G., Taylor, T.J., Thomas, O.M., Tustison, N.J., Unal, G., Vasseur, F., Wintermark, M., Ye, D.H., Zhao, L., Zhao, B., Zikic, D., Prastawa, M., Reyes, M., Van Leemput, K.: The Multimodal Brain Tumor Image Segmentation Benchmark (BRATS). *IEEE Transactions on Medical Imaging* **34**(10), 1993–2024 (2015). <https://doi.org/10.1109/TMI.2014.2377694>
6. Bakas, S., Akbari, H., Sotiras, A., Bilello, M., Rozycki, M., Kirby, J., Freymann, J., Farahani, K., Davatzikos, C.: Advancing The Cancer Genome Atlas glioma MRI collections with expert segmentation labels and radiomic features. *Scientific Data* **4** (09 2017). <https://doi.org/10.1038/sdata.2017.117>

7. Bakas, S., Akbari, H., Sotiras, A., Bilello, M., Rozycki, M., Kirby, J., Freymann, J., Farahani, K., Davatzikos, C.: Segmentation Labels and Radiomic Features for the Pre-operative Scans of the TCGA-GBM collection (07 2017). <https://doi.org/10.7937/K9/TCIA.2017.KLXWJJ1Q>
8. Ronneberger, O., Fischer, P., Brox, T.: U-Net: Convolutional Networks for Biomedical Image Segmentation. In: Navab, N., Hornegger, J., Wells, W.M., Frangi, A.F. (eds.) *Medical Image Computing and Computer-Assisted Intervention – MICCAI 2015*. pp. 234–241. Springer International Publishing, Cham (2015)
9. Myronenko, A.: 3D MRI Brain Tumor Segmentation Using Autoencoder Regularization. In: Crimi, A., Bakas, S., Kuijf, H., Keyvan, F., Reyes, M., van Walsum, T. (eds.) *Brainlesion: Glioma, Multiple Sclerosis, Stroke and Traumatic Brain Injuries*. pp. 311–320. Springer International Publishing, Cham (2019)
10. Jiang, Z., Ding, C., Liu, M., Tao, D.: Two-Stage Cascaded U-Net: 1st Place Solution to BraTS Challenge 2019 Segmentation Task. In: Crimi, A., Bakas, S. (eds.) *Brainlesion: Glioma, Multiple Sclerosis, Stroke and Traumatic Brain Injuries*. pp. 231–241. Springer International Publishing, Cham (2020)
11. Isensee, F., Jäger, P.F., Kohl, S.A., Petersen, J., Maier-Hein, K.H.: nnU-Net: a self-configuring method for deep learning-based biomedical image segmentation. pp. 1–9. *Nature Methods* (2020)
12. Isensee, F., Jäger, P.F., Full, P.M., Vollmuth, P., Maier-Hein, K.H.: nnU-Net for Brain Tumor Segmentation. In: Crimi, A., Bakas, S. (eds.) *Brainlesion: Glioma, Multiple Sclerosis, Stroke and Traumatic Brain Injuries*. pp. 118–132. Springer International Publishing, Cham (2021)
13. NVIDIA nnU-Net implementation. <https://github.com/NVIDIA/DeepLearningExamples/tree/master/PyTorch/Segmentation/nnUNet>, accessed: 2021-09-30
14. Cox, R., Ashburner, J., Breman, H., Fissell, K., Haselgrove, C., Holmes, C., Lancaster, J., Rex, D., Smith, S., Woodward, J., Strother, S.: A (sort of) new image data format standard: NiFTI-1. vol. 22 (01 2004)
15. Hatamizadeh, A., Yang, D., Roth, H., Xu, D.: UNETR: Transformers for 3D Medical Image Segmentation (2021)
16. Dosovitskiy, A., Beyer, L., Kolesnikov, A., Weissenborn, D., Zhai, X., Unterthiner, T., Dehghani, M., Minderer, M., Heigold, G., Gelly, S., Uszkoreit, J., Houlsby, N.: An image is worth 16x16 words: Transformers for image recognition at scale (2021)
17. Vaswani, A., Shazeer, N., Parmar, N., Uszkoreit, J., Jones, L., Gomez, A.N., Kaiser, L., Polosukhin, I.: Attention is all you need (2017)
18. Kingma, D.P., Welling, M.: Auto-encoding variational bayes (2014)
19. Zhu, Q., Du, B., Turkbey, B., Choyke, P.L., Yan, P.: Deeply-supervised cnn for prostate segmentation (2017)
20. Oktay, O., Schlemper, J., Folgoc, L.L., Lee, M., Heinrich, M., Misawa, K., Mori, K., McDonagh, S., Hammerla, N.Y., Kainz, B., Glocker, B., Rueckert, D.: Attention u-net: Learning where to look for the pancreas (2018)
21. He, K., Zhang, X., Ren, S., Sun, J.: Deep residual learning for image recognition (2015)
22. Ghiasi, G., Lin, T.Y., Le, Q.V.: Dropblock: A regularization method for convolutional networks (2018)
23. Tsung-Yi Lin, Priya Goyal, Ross Girshick, Kaiming He, Piotr Dollár: Focal Loss for Dense Object Detection. *International Conference on Computer Vision (ICCV)* (2017)

24. Fausto Milletari, Nassir Navab, Seyed-Ahmad Ahmadi: V-Net: Fully Convolutional Neural Networks for Volumetric Medical Image Segmentation. International Conference on 3D Vision (3DV) (2016)
25. Paszke, A., Gross, S., Massa, F., Lerer, A., Bradbury, J., Chanan, G., Killeen, T., Lin, Z., Gimelshein, N., Antiga, L., Desmaison, A., Kopf, A., Yang, E., DeVito, Z., Raison, M., Tejani, A., Chilamkurthy, S., Steiner, B., Fang, L., Bai, J., Chintala, S.: Pytorch: An imperative style, high-performance deep learning library. In: Wallach, H., Larochelle, H., Beygelzimer, A., d'Alché-Buc, F., Fox, E., Garnett, R. (eds.) Advances in Neural Information Processing Systems 32, pp. 8024–8035. Curran Associates, Inc. (2019), <http://papers.neurips.cc/paper/9015-pytorch-an-imperative-style-high-performance-deep-learning-library.pdf>
26. Micikevicius, P., Narang, S., Alben, J., Diamos, G., Elsen, E., Garcia, D., Ginsburg, B., Houston, M., Kuchaiev, O., Venkatesh, G., Wu, H.: Mixed precision training (2018)
27. Kingma, D.P., Ba, J.: Adam: A method for stochastic optimization (2017)
28. Loshchilov, I., Hutter, F.: Sgdr: Stochastic gradient descent with warm restarts (2017)
29. Antonelli, M., Reinke, A., Bakas, S., Farahani, K., AnnetteKopp-Schneider, Landman, B.A., Litjens, G., Menze, B., Ronneberger, O., Summers, R.M., van Ginneken, B., Bilello, M., Bilic, P., Christ, P.F., Do, R.K.G., Gollub, M.J., Heckers, S.H., Huisman, H., Jarnagin, W.R., McHugo, M.K., Napel, S., Pernicka, J.S.G., Rhode, K., Tobon-Gomez, C., Vorontsov, E., Huisman, H., Meakin, J.A., Ourselin, S., Wiesenfarth, M., Arbelaez, P., Bae, B., Chen, S., Daza, L., Feng, J., He, B., Isensee, F., Ji, Y., Jia, F., Kim, N., Kim, I., Merhof, D., Pai, A., Park, B., Perslev, M., Rezaifar, R., Rippel, O., Sarasua, I., Shen, W., Son, J., Wachinger, C., Wang, L., Wang, Y., Xia, Y., Xu, D., Xu, Z., Zheng, Y., Simpson, A.L., Maier-Hein, L., Cardoso, M.J.: The Medical Segmentation Decathlon (2021)